Nuclear Materials and Energy 15 (2018) 55–63

Contents lists available at ScienceDirect

Nuclear Materials and Energy

journal homepage: www.elsevier.com/locate/nme

Adhesive force distributions for tungsten dust deposited on bulk tungsten and beryllium-coated tungsten surfaces

P. Tolias[*,a], G. Riva[b], M. De Angeli[c], S. Ratynskaia[a], G. Daminelli[b], C.P. Lungu[d], C. Porosnicu[d]

[a] Space and Plasma Physics, KTH Royal Institute of Technology, Teknikringen 31, Stockholm 10044, Sweden
[b] Institute of Condensed Matter Chemistry and Energy Technologies, Consiglio Nazionale delle Ricerche, via Cozzi 53, Milan 20125, Italy
[c] Istituto di Fisica del Plasma, Consiglio Nazionale delle Ricerche, via Cozzi 53, Milan 20125, Italy
[d] National Institute for Laser, Plasma and Radiation Physics (NILPRP), Magurele-Bucharest 077125, Romania

ABSTRACT

Comprehensive measurements of the adhesive force for tungsten dust adhered to tungsten surfaces have been performed with the electrostatic detachment method. Monodisperse spherical dust has been deposited with gas dynamics techniques or with gravity mimicking adhesion as it naturally occurs in tokamaks. The adhesive force is confirmed to follow the log-normal distribution and empirical correlations are proposed for the size-dependence of its mean and standard deviation. Systematic differences are observed between the two deposition methods and attributed to plastic deformation during sticking impacts. The presence of thin beryllium coatings on tungsten surfaces is demonstrated to barely affect adhesion.

1. Introduction

Tokamak-generated dust has been considered to be a key plasma-wall interaction issue for ITER, where it can pose a safety risk during accidental scenarios, constitute an operational hazard in case of strong penetration in the burning plasma, lead to degradation of in-vessel diagnostics or inspection tools and compromise the thermomechanical integrity of castellated plasma-facing components by bridging the gaps [1–6]. Adhesion has been acknowledged to have a pivotal role in many physical and technical aspects of tokamak dust such as mechanical impacts with plasma-facing-components [7–9], remobilization by steady state plasmas and edge-localized modes [10–12], resuspension during loss-of-vacuum accidents [13,14], the efficiency of post-mortem collection activities [15–17] as well as the development of in-situ removal techniques [18,19]. Owing to insurmountable difficulties in the first-principle quantification of adhesion between technical (rough, polycrystalline, adsorbate covered) surfaces, accurate adhesive force measurements are imperative [20,21].

The first systematic measurements of the adhesive force for μm-sized fusion relevant dust have been recently carried out with the electrostatic detachment method [20]. In particular, the experiments involved nearly monodisperse spherical tungsten dust populations that were adhered to planar tungsten surfaces in a controlled manner. The adhesive force was revealed to behave as a stochastically distributed random variable with a mean value that is approximately two orders of magnitude smaller than the predictions of contact mechanics models, but in strong agreement with the van der Waals formula. The above observations were explained by considering the omnipresent effect of nanometer-scale surface roughness for stiff materials such as tungsten. However, only the mean adhesive force was determined [20] and not the cumulative probability distribution of the adhesive force, which constitutes the primary external input for the theoretical modelling of adhesion in dust remobilization and resuspension problems.

In this work, comprehensive measurements of the tungsten on tungsten (W-on-W) adhesive force distribution are reported that have been carried out with the electrostatic detachment method. Three nearly monodisperse spherical W dust populations (6 μm, 9 μm, 14 μm) have been adhered to planar W substrates of varying surface roughness ($R_{q,s} \sim 10 - 100$ nm) with two different deposition methods. The gas-assisted deposition attempts to mimic adhesion to the first wall and divertor during tokamak discharges, whereas the gravity assisted deposition attempts to mimic adhesion to the vessel floor after discharge termination. Benefitting from the unprecedented statistics, the general form of the adhesive force distribution is determined as well as empirical correlations are proposed that describe the size-dependence of the mean and standard deviation of the adhesive force. Systematic differences in the adhesive force achieved with the two deposition methods are pointed out and their physical origin is discussed.

In addition, comprehensive measurements of the tungsten on beryllium-coated tungsten (W-on-Be/W) adhesive force distribution with

* Corresponding author.
E-mail address: tolias@kth.se (P. Tolias).

https://doi.org/10.1016/j.nme.2018.05.013
Received 24 January 2018; Received in revised form 25 March 2018; Accepted 15 May 2018

the electrostatic detachment method are reported. High density Be films of varying thickness ($\delta = 10, 100, 1000$ nm) have been deposited on W substrates with the thermionic vacuum arc method. Subsequently, two nearly monodisperse spherical W dust populations (9 μm, 14 μm) have been adhered to the coated substrates with gravity-assisted deposition. The adhesion of the W-on-Be/W and W-on-W systems is compared.

2. Experimental aspects

2.1. Underlying physics of the measurement technique

In the electrostatic detachment method, a high dc potential difference ΔV is applied between two parallel plate electrodes with the metallic dust adhered to the grounded electrode. In this manner, a normal-to-the-electrode electrostatic force is exerted on the grains tending to detach them from the substrate. For spherical perfectly conducting grains, provided that the inter-electrode spacing d is much larger than the dust diameter, the electrostatic force is described by the so-called Lebedev formula [22]

$$F_e = k_D E^2 D_d^2 \ (\mu N), \tag{1}$$

with E the electrostatic field strength in kV/mm, D_d the dust diameter in μm and the proportionality constant given by $k_D = 0.38 \times 10^{-4} (\mu N mm^2)/(kV^2 \mu m^2)$. This expression is exact for $d \gg D_d$ and stems from the solution of the Laplace equation for a spherical conductor in contact with a grounded plane in presence of a uniform normal electrostatic field. As such, the Lebedev formula self-consistently accounts for the infinite set of image charges [23]. To be more precise, the potential field is found with the aid of degenerate bi-spherical coordinates and the force is calculated by integrating the electrostatic stress over the surface of the sphere. Note that for a sufficiently small inter-electrode spacing (of the order few dust sizes), the local electrostatic field would be affected by the presence of dust and the Lebedev formula would no longer be valid.

When all other non-contact normal forces are negligible, the electrostatic force just needs to exceed the adhesive force or pull-off force for dust to be detached, $F_e \geq F_{po}$. Hence, the adhesive force can be indirectly measured by slowly increasing the applied electrostatic field $E = \Delta V/d$ until the detachment condition is satisfied. Other normal forces in action are of dielectrophoretic, capillary, aerodynamic and gravitational nature: **(i)** Dust is always deposited near the symmetry axis of the parallel plate cylindrical capacitor, where fringing effects are minimized leading to highly uniform electrostatic fields. As a result, *dielectrophoretic forces* arising due to electrostatic field gradients [24] are negligible. **(ii)** The experiments are always performed under high vacuum conditions (< 0.05 Pa). The main reason is to prevent the applied electrostatic fields (up to ~ 60 kV/mm) from causing dielectric breakdown of the ambient gas. However, low pressures also strongly decrease adsorbed humidity due to evaporation. Thus, *capillary forces* due to condensed water molecules should be weak [25]. **(iii)** Vacuum is broken between measurements by dry nitrogen puffing through a narrow orifice (~ 30 cm from the chamber). Along the orifice tube, a valve is placed that further reduces the flow conductance. Moreover, the chamber-end of the orifice tube is not in direct view of the grounded electrode. These imply that *aerodynamic forces* arising during pumping to atmospheric pressures should be negligible. This is indirectly confirmed by the lowest electrostatic field (1.5 kV/mm) measurements which never led to any dust detachment. **(iv)** For $D_d = 20$ μm spherical tungsten dust, the *gravitational force* is merely of the order of nN, whereas the adhesive force is of the order of μN. Gravity is clearly negligible at least up to $D_d = 200$ μm.

2.2. Description of the experimental procedure

The parallel plate capacitor consists of two cylindrical electrodes of 20 mm diameter. The upper dust-free electrode was made of stainless steel or brass and its bottom face was sprayed with a ~ 40 μm acrylic layer in order to prevent the re-deposition of detached dust grains [20,26]. The bottom dust-loaded electrode featured a hollow stainless steel or brass cylinder where the pure or beryllium-coated tungsten substrate containing the deposited dust was adjusted. The maximum voltage difference supplied was 25 kV and the inter-electrode spacing was $d = 0.5 - 1$ mm resulting to a maximum electrostatic field of 50 kV/mm. In few occasions, such fields did not suffice to mobilize all adhered dust and the inter-electrode spacing had to be set to $d = 0.25$ mm. However, electrostatic fields higher than 60 kV/mm were not possible due to dielectric breakdown.

After deposition, the dust-loaded substrate is inserted in the bottom electrode which is mounted in the capacitor. The system is pumped down to low pressures. A 1.5 kV potential difference is applied and maintained for several minutes. Vacuum is broken, the bottom electrode is removed and images are taken by an optical microscope. The procedure is repeated with a slightly higher electrostatic field until all dust has been removed or dielectric breakdown has occurred. The images corresponding to adjacent electrostatic field values are overlaid and the number of isolated grains mobilized during each exposure is determined. Clusters are identified and excluded from counting.

2.3. Dust composition, size and morphology

The W dust employed was supplied by “TEKNA Advanced Materials Inc” and produced by a radio frequency inductively coupled plasma torch operating with high purity argon under atmospheric pressure [27]. The process is based on melting of precursor irregular W powder inside the plasma volume and free-fall resolidification of the resulting droplets inside a quenching volume prior to collection [28].

This dust production technique has numerous advantages in view of tokamak applications: **(i)** The plasma residence time is enough for the W droplets to be spheroidized by surface tension leading to dust with a mean sphericity $> 95\%$ [29,30]. As we shall see, this permits the use of the Lebedev and van der Waals formulas. **(ii)** Melting followed by resolidification should also occur for tokamak-generated dust passing through the edge plasma and ending up in magnetically shadowed regions as well as for disruption-generated dust passing through the shrinking plasma and ending up in the mitigating gas volume. Such a sequence leads to dust densification, *i.e.* low internal porosities and high mass densities [28]. **(iii)** The electrode-less operation and the vaporization of volatile contaminants lead to very high purity levels $> 99.9\%$. The absence of an oxidizing environment and the possibility of chemical desorption at elevated temperatures ensure an ultra low oxygen content ~ 100 ppm [30]. Thus, dust exhibits an excellent electrical conductivity and cannot sustain charges when in contact with other metallic surfaces.

The nominal size distribution was 5-25 μm with an average diameter of ~ 10 μm, but scanning electron microscope (SEM) analysis revealed the presence of few smaller dust grains down to ~ 3 μm. SEM analysis also revealed a very low fraction of small ~ 5 μm non-spherical grains; most probably precursor powder that was not melted by the plasma torch being optically shadowed by the incident heat flux. From this polydisperse batch, nearly monodisperse subpopulations were meshed out with the aid of high precision electroformed nickel sieves and ultrasonic cells. The targeted diameters were 6, 9, 14 μm. Comparing with W dust produced in contemporary tokamaks; in AUG collected spherical W-dominated dust had a most probable diameter of 1-2 μm and a 50 μm maximum diameter [15], whereas in JET-ILW only few W particulates were collected with characteristic sizes ~ 10 μm [16].

The root-mean-square roughness of the dust surface was not measured directly. Nevertheless, zoomed-in SEM inspection and comparison with well-characterized mirror-polished planar W samples led us to conclude that $R_{q,\,d} \lesssim 20$ nm for typical grains. On rather rare occasions,

ultra-fine W powder had been attached to the dust surface leading to $R_{q,d} \lesssim 100$ nm. This could stem from enhanced W vapor condensation in some regions of the plasma torch and has been previously documented [31]. Overall, an average dust roughness $R_{q,d} \sim 20$ nm can be assumed.

2.4. Substrate composition and roughness

The pure W substrates were cylindrical with a diameter varying from 6 mm to 10 mm. Six different substrates were employed in order to avoid any bias arising due to chemical and energetic heterogeneities. The roughness characterizing the whole substrate area was measured by a surface profiler, the root-mean-square metric varied in the range $R_{q,s} \simeq 12 - 104$ nm (11.9, 21.8, 31.6, 73.4, 100.4, 104.2 nm). The roughness characterizing the central dust deposition areas was measured by atomic force microscopy, the root-mean-square metric varied in the range $R_{q,s} \sim 8 - 134$ nm. The rms roughness characterizing different deposition areas of the same substrate exhibited variations of the order of 40%. Exposure to high electrostatic fields barely altered the surface roughness, since the arc path during dielectric breakdown closed on the adhered dust grains.

The beryllium-coated W substrates were cylindrical with a 10 mm diameter. Three different W substrates were employed owing to the three targeted Be film thicknesses. To reduce the risk of inhomogeneous film growth, the substrates were initially mirror polished. Prior to the coating, the roughness of the whole substrates and the deposition areas was $R_{q,s} \sim 20$ nm, exhibiting $\sim 50\%$ variations. The beryllium films were manufactured at the National Institute of Laser, Plasma and Radiation in Romania with the thermionic vacuum arc method [32,33]. High density layers with bulk-like properties and varying $\delta = 10, 100, 1000$ nm thickness were produced. Limited-in-extent contaminated regions were observed near the stainless steel - tungsten interface, but influenced neither the overall film properties nor the detachment measurements, since these regions lie at the edge of the W insert away from the central dust deposition areas. Coating barely altered the surface roughness, whose rms values became 17 nm ($\delta = 10$ nm), 25 nm ($\delta = 100$ nm), 26 nm ($\delta = 1000$ nm).

2.5. Dust deposition

W dust was deposited into circular deposition areas of 0.3 mm diameter, hereafter referred to as dust spots. Each substrate contained either 5 or 9 spots. The 5−spot substrates featured a central spot and four spots 2 mm from the center. The 9−spot substrates featured a central spot, four spots 1.4 mm from the center and four spots 2.8 mm from the center. Optical images of a dust spot after its exposure to two successive high electrostatic fields are presented in Fig. 1. Despite the local roughness variations, the asymmetries in the mobilized dust fraction between different spots of the same substrate were always observed to be of reasonable extent, as expected from the homogeneity of the applied field.

Two different deposition methods were employed. In the *gas-assisted* deposition method, the dust grains are aerodynamically launched against gravity towards the substrate with impact velocities below the sticking threshold [10]. In order to minimize the number of agglomerates, the mediated variant of this deposition method was preferred [10,20], where dust is preemptively loaded on 4 mm plastic spheres which collide with a 2 m/s speed on a protective mask that is placed right above the substrate. The mask bears 0.5 mm thick holes of 0.3 mm diameter (reflecting the dust deposition area). The impact of the carrier leads to an impulsive acceleration of the loaded dust which is detached towards the mask. Some of the released dust grains free stream through the holes and stick to the substrate, whereas the remaining grains rebound on the mask. This method has been argued to realistically mimic dust adhesion to the first wall and divertor as it naturally occurs during tokamak discharges [10], where, due to the curved plasma flow, centrifugal effects arising from the typically dominant ion drag force make mechanical collisions with plasma-facing components unavoidable. In the *gravity-assisted* deposition method, a thin brush is immersed in the dust container and then gently stroked slightly above the substrate. The tribo-statically sampled dust is softly accelerated by gravity towards the substrate, where it ultimately adheres after a single or multiple impacts. The average impact speed is ~ 0.5 m/s. This method attempts to mimic dust adhesion to the vessel floor as it occurs after the termination of tokamak discharges, where plasma-induced forces cease and motion becomes free falling.

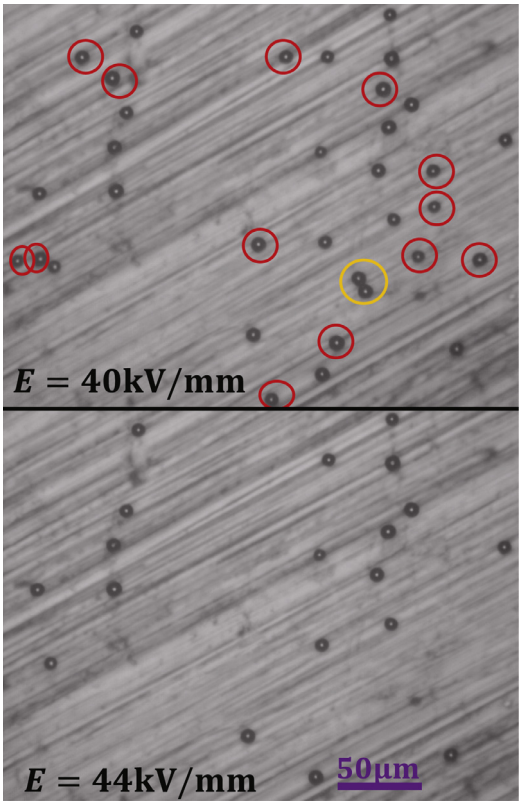

Fig. 1. Nearly monodisperse 9 μm W dust adhered to a pure W substrate of 104.2 nm rms roughness containing five dust spots deposited with the gas-assisted method. Optical images of the central dust spot after exposure to two successive electrostatic fields, $E = 40$ kV/mm and $E = 44$ kV/mm. The application of $E = 44$ kV/mm led to the detachment of 13 isolated grains (red circles) and one doublet (orange circle). The small cluster has not been considered in the mobilized fraction. It is evident that the use of multiple small spots facilitates particle counting without compromising statistics. (For interpretation of the references to colour in this figure legend, the reader is referred to the web version of this article.)

3. Adhesive force distributions for tungsten dust deposited on tungsten substrates

3.1. The concept of adhesive force distributions

In ideal situations, where a spherical homogeneous smooth dust grain is attached to a planar homogeneous smooth substrate, the adhesive force should acquire a unique well-defined value since adhesion is a deterministic phenomenon. In practical situations, owing to the statistical character of surface roughness at the nanometer scale of the contact area (structural heterogeneity) as well as the random coverage by surface adsorbates (chemical heterogeneity) and the random orientation of micro-crystallites (energetic heterogeneity), the adhesive force is better described in probabilistic terms. As a consequence, adhesion cannot be determined by the minimum normal force required for dust removal but by the dust removal probability associated with a

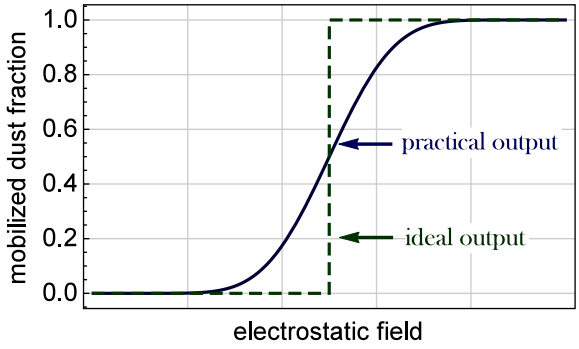

Fig. 2. Schematic of the characteristic raw output of adhesion measurements with the electrostatic detachment method; ideal situation in the absence of structural, chemical and energetic heterogeneities (dashed line), practical situation in the presence of heterogeneities and other experimental uncertainties (solid line).

given normal force magnitude. This has been systematically concluded by numerous adhesion measurements carried out with the colloidal probe method of atomic force microscopy [25,34], the centrifuge detachment method [35,36] and the electrostatic detachment method [26,37].

Let us now discuss how the probabilistic nature of adhesion manifests itself in measurements with the electrostatic detachment method. The direct output of such experiments comprises of the mobilized dust number versus the externally applied electrostatic field. Ideally, the curve would have the form of a Heaviside-step function with the discontinuity jump occurring at the electrostatic field for which the applied normal force equals the unique adhesive force [20]. Practically, the curve has a sigmoid function form, since the transition from no removal to complete detachment is gradual and occurs over an extended range of electrostatic fields. This sigmoid-type deviation from the step function, illustrated in Fig. 2, is mainly caused by the aforementioned omnipresent heterogeneities.

The mobilized number versus electrostatic field curves can be converted into mobilized fraction versus applied extraction force curves through the Lebedev formula. These curves are essentially cumulative probability distributions revealing the fraction of dust with adhesive forces smaller than a given value and their first derivative yields the probability density. As accustomed in the literature [38–40], the adhesive force shall be assumed to be log-normally distributed. The probability density and the cumulative probability distributions shall follow the expressions [41]

$$\phi(F_{po}) = \frac{1}{\sqrt{2\pi}}\frac{1}{aF_{po}}\exp\left[-\frac{(\ln F_{po}-b)^2}{2a^2}\right], \quad (2)$$

$$\Phi(F_{po}) = \frac{1}{2}\mathrm{erfc}\left(-\frac{\ln F_{po}-b}{\sqrt{2}\,a}\right), \quad (3)$$

respectively, where erfc(.) denotes the complementary error function. The mean (μ) and standard deviation (σ) of the adhesive force are then given by [41]

$$\mu = e^{b+\frac{1}{2}a^2}, \quad (4)$$

$$\sigma = e^{b+\frac{1}{2}a^2}\sqrt{e^{a^2}-1}\,. \quad (5)$$

The unknown parameters a, b will be found by least-square fitting the experimental cumulative probability to Eq. (3).

Unavoidably, the measurements are also affected by limitations concerning the finite spread of the dust size distributions, the discrete step increase of the applied voltage difference, the formation of agglomerates during deposition, uncertainties in the inter-electrode spacing, departures from perfect dust sphericity and contact area variations caused by plastic deformation during impact. As discerned from Section 2, considerable effort has been taken to ensure that these uncertainties are minimized (dust size variations, non-sphericity) or even eliminated (agglomerates). Clearly, some of these limitations cannot be exactly quantified and translated into measurement uncertainties. The experimental error in the adhesive force due to uncertainties in the inter-electrode spacing and the optical resolution of the size distribution has been computed, see Figs. 3–5. It is maximized at the highest force values where the cumulative probability is nearly unity, implying that the determination of a, b and thus of μ, σ is robust.

3.2. Motivation and measured adhesive force distributions

It is not only formidable but also meaningless to quantify the adhesive force for fusion relevant dust-substrate combinations as a function of the rms roughness: **(i)** The characterization of the surface roughness of any macroscopic substrate by the typical rms metric only determines the average value of the largest roughness length scale. However, adhesion is determined by the multi-scale roughness features beneath each dust-substrate contact area. **(ii)** Both adhering bodies are characterized by finite roughness and the local interface topology should change (at least for the softer body) due to plastic deformation during sticking impacts. **(iii)** In fusion devices, intense plasma-surface interactions should lead to time-dependent spatially varying roughness profiles which are not accessible to modelers.

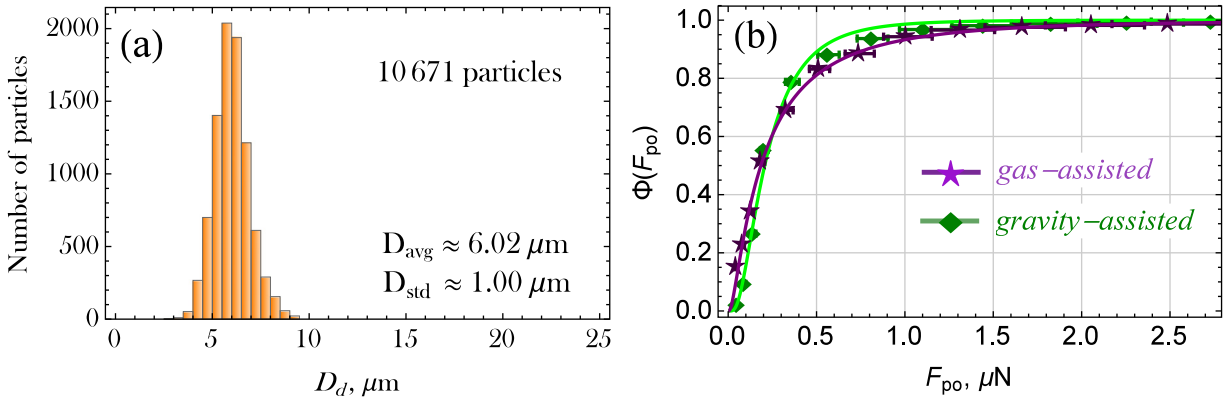

Fig. 3. Nearly monodisperse 6 μm W dust on bulk W substrates. (a) Histogram of the size distribution of the adhered dust as determined from the optical microscope, the mean and standard deviation of the diameter are also provided. (b) The experimental cumulative probability distribution of the adhesive force (discrete points owing to the stepwise increase of the mobilizing electrostatic field) together with the least-square fitted log-normal cumulative probability (solid line) for gas-assisted and gravity-assisted deposition. The horizontal error bars stem from the 25 μm uncertainty in the inter-electrode spacing $d = 0.5$ mm or $d = 1.0$ mm and the 0.5 μm uncertainty in the dust diameters.

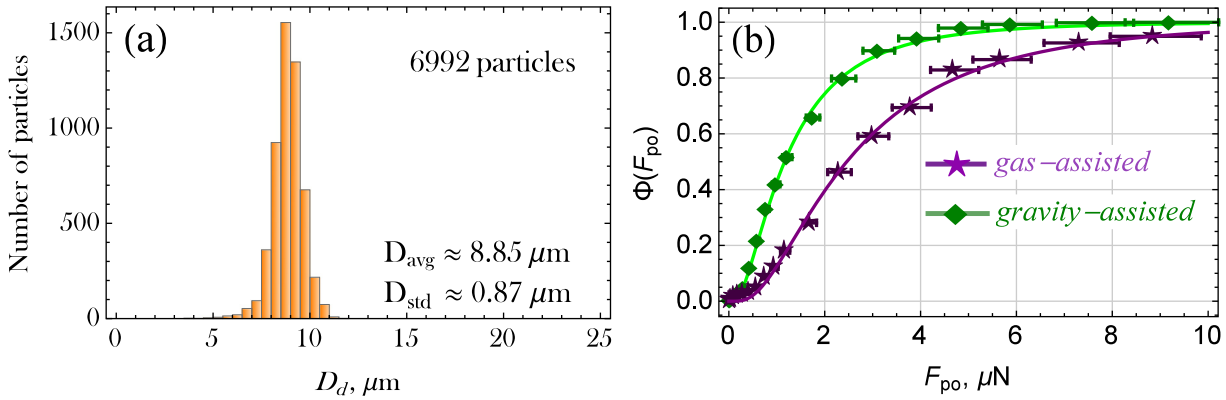

Fig. 4. Nearly monodisperse 9 μm W dust on bulk W substrates. (a) Histogram of the size distribution of the adhered dust as determined from the optical microscope, the mean and standard deviation of the diameter are also provided. (b) The experimental cumulative probability distribution of the adhesive force (discrete points owing to the stepwise increase of the mobilizing electrostatic field) together with the least-square fitted log-normal cumulative probability (solid line) for gas-assisted and gravity-assisted deposition. The horizontal error bars stem from the 25 μm uncertainty in the inter-electrode spacing $d = 0.5$ mm or $d = 1.0$ mm and the 0.5 μm uncertainty in the dust diameters.

Nevertheless, it is important for practical applications to quantify adhesion for a wide range of roughness values. Provided that the rms metric exceeds few nanometers so that metallic bonding interactions are not relevant (which would manifoldly increase adhesion), the rms roughness is smaller than the dust-substrate contact radius (~ 1 μm in case of D_d ~ 10 μm W) so that a single contact area is established and a unique surface normal is defined, then the mean adhesive force can be expected to weakly depend on the rms roughness, whose variations will mainly affect the spread of the adhesive force. In fact, this was suggested by our previous experiments [20]. An *effective rms roughness* that characterizes both adhering bodies can be defined by $R_{q,eff}^2 = R_{q,s}^2 + R_{q,d}^2$ when assuming non-conforming surfaces and neglecting impact-induced plasticity, which leads to $R_{q,eff} = 22 - 135$ nm for the dust and substrate rms roughness ranges provided in Sections 2.3 and 2.4.

W-on-W adhesion measurements have been carried out for three monodisperse dust populations and two deposition methods constituting six measurement sets. Six substrates were employed and the adhesive force distributions were representative of $R_{q,eff} = 22 - 135$ nm. In order to enable an unbiased comparison between the different dust sizes and deposition methods, an *equivalent rms substrate roughness* $R_{q,eq}$ for each measurement set was defined by the arithmetic average of each substrate roughness weighed by the relative number of detached dust grains and precautions were taken to keep its value: (1) nearly constant in order to ensure that the rms roughness range was sampled in an approximately similar manner for each measurement set, (2) as close as possible to the value $(\min\{R_{q,s}\} + \max\{R_{q,s}\})/2 \simeq 58$ nm in order to ensure that the rms roughness range was sampled in an approximately uniform manner.

Nearly monodisperse 6μm dust. $N = 10671$ dust grains were detached, whose size distribution is illustrated in Fig. 3(a); the mean dust diameter is $D_{avg} \simeq 6.02$ μm which is nearly identical to the targeted size of $D_{nom} = 6$ μm. Gas-assisted deposition concerned $N = 3056$ grains with $D_{avg} \simeq 5.82$ μm and $R_{q,\ eq} \simeq 47$ nm. Gravity-assisted deposition concerned $N = 7615$ grains with $D_{avg} \simeq 6.1$ μm and $R_{q,\ eq} \simeq 56$ nm.
Nearly monodisperse 9 μm dust. $N = 6992$ dust grains were detached, whose exact size distribution is illustrated in Fig. 4(a); the mean dust diameter is $D_{avg} \simeq 8.85$ μm which is very close to the targeted size of $D_{nom} = 9$ μm. Gas-assisted deposition concerned $N = 3880$ grains with $D_{avg} \simeq 8.78$ μm and $R_{q,\ eq} \simeq 46$ nm, whereas gravity assisted deposition concerned $N = 3112$ grains with $D_{avg} \simeq 8.94$ μm and $R_{q,eq} \simeq 51$ nm.
Nearly monodisperse 14 μm dust. $N = 1654$ dust grains were detached, whose exact size distribution is illustrated in Fig. 5(a); the mean dust diameter is $D_{avg} \simeq 14.40$ μm which is close to the targeted size of $D_{nom} = 14$ μm. Gas-assisted deposition concerned $N = 940$ grains with $D_{avg} \simeq 14.07$ μm and $R_{q,eq} \simeq 66$ nm, whereas gravity-assisted deposition concerned $N = 714$ grains with $D_{avg} \simeq 14.82$ μm and $R_{q,eq} \simeq 53$ nm.

Regardless of the monodisperse population and the deposition method, the experimental cumulative probability distribution verified

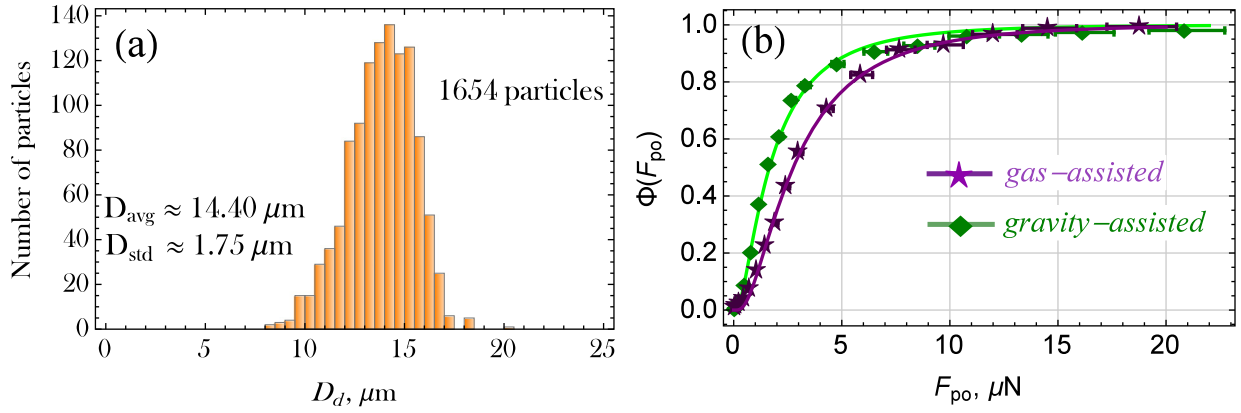

Fig. 5. Nearly monodisperse 14 μm W dust on bulk W substrates. (a) Histogram of the size distribution of the adhered dust as determined from the optical microscope, the mean and standard deviation of the diameter are also provided. (b) The experimental cumulative probability distribution of the adhesive force (discrete points owing to the stepwise increase of the mobilizing electrostatic field) together with the least-square fitted log-normal cumulative probability (solid line) for gas-assisted and gravity-assisted deposition. The horizontal error bars stem from the 25 μm uncertainty in the inter-electrode spacing $d = 0.5$ mm or $d = 1.0$ mm and the 0.5 μm uncertainty in the dust diameters.

Table 1
Experimental results for the mean and spread of the adhesive force obtained for different nearly monodisperse populations of spherical W dust adhered to bulk planar W substrates with the use of different deposition methods.

Mean value μ (μN)		
D_{nom}	Gas-assisted	Gravity-assisted
6 μm	0.349	0.267
9 μm	3.339	1.639
14 μm	3.856	2.527
Standard deviation σ (μN)		
D_{nom}	Gas-assisted	Gravity-assisted
6 μm	0.559	0.219
9 μm	3.068	1.629
14 μm	3.783	2.924

that the adhesive force behaves as a log-normally distributed random variable, see Figs. 3(b),4(b) and 5(b). The least square fit results for the mean and spread of the adhesive force (μ, σ) for each combination of monodisperse dust population and deposition method are presented in Table 1.

3.3. Comparison of the mean adhesive force with the van der Waals formula

In our previous work [20], it was concluded that the mean W-on-W adhesive force is nearly two orders of magnitude smaller than the predictions of contact mechanics models but in strong agreement with the predictions of the van der Waals formula. It was argued that, as a consequence of the omnipresent nano-roughness, adhesion is not determined by short-range electron exchange interactions of the metallic bonding type (with an associated surface energy of the order of 5 J/m^2) but by weaker longer-range interactions between instantaneously induced multipoles (with an associated surface energy of the order of 0.1 J/m^2) [42]. For spherical dust of diameter D_d in the proximity of a planar surface, the van der Waals formula reads as [43–45]

$$F_{VdW} = \frac{A}{12 z_0^2} D_d \,. \tag{6}$$

The values employed for the non-retarded Hamaker constant A and distance of closest approach z_0 have been revised compared to our previous work where $A = 4 \times 10^{-19}$ J and $z_0 = 0.3$ nm was considered [20]. Recent Lifshitz theory calculations employing extensive dielectric data and following two independent computational methods led to the recommendation $A = 4.98 \times 10^{-19}$ J for W-on-W [46], whereas the distance of closest approach should exceed the metallic bond range of ~ 0.3 nm [45] leading to the use of $z_0 = 0.4$ nm [42,45]. Overall, the material dependent pre-factor $A/(12 z_0^2)$ decreased from 0.37 J/m^2 to 0.26 J/m^2, which does not alter the main conclusions of Ref. [20].

It is possible to calculate the mean adhesive force directly from the raw experimental output without utilizing probability distribution functions [20]. Let M be the number of distinct externally applied electrostatic field values, N be the total number of adhered dust grains, N_i be the number of dust grains detached by the $i-$th applied voltage difference with $F_{po,i} = F_{e,i}$ the associated electrostatic force as described by the Lebedev formula. Then the mean adhesive force can be estimated by the *discrete expression*

$$\overline{F}_{po} = \sum_{i=1}^{M} \left[\left(\frac{N_i}{N} \right) F_{po,i} \right] / \sum_{i=1}^{M} \left(\frac{N_i}{N} \right). \tag{7}$$

The denominator can be smaller than unity, when dielectric breakdown takes place prior to the detachment of all adhered dust grains. The drawbacks of this expression are connected to the dependence on the finite discrete voltage-difference steps and the rather ad-hoc compensation in the case of premature dielectric breakdown.

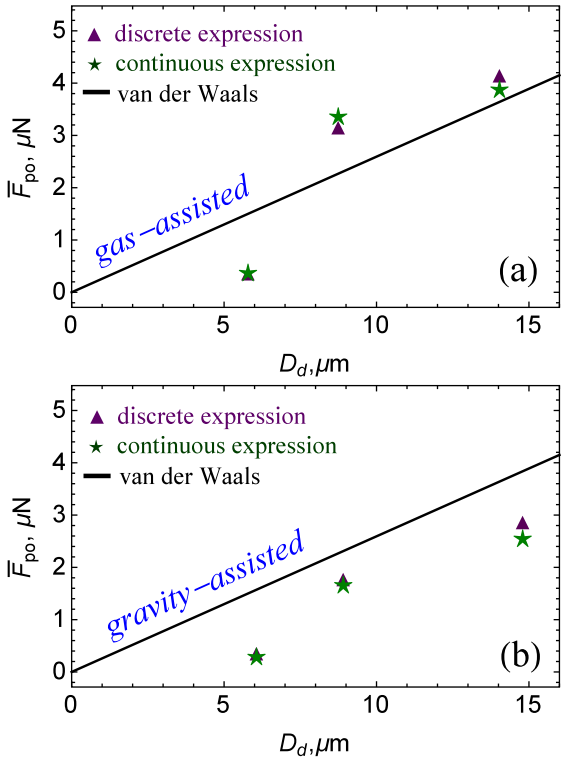

Fig. 6. The mean adhesive force for spherical W dust deposited on planar bulk W substrates of varying surface roughness as a function of the dust diameter. Theoretical values according to the van der Waals formula [solid line, see Eq. (6)], experimental values according to the discrete expression [▲ symbols, see Eq. (7)], experimental values according to the continuous expression [⋆ symbols, see Eq. (8)]. Results for deposition by (a) gas dynamics techniques, (b) gravity. The $\overline{F}_{po}$ experimental uncertainties are too small to be depicted on the graph in a meaningful manner: the relative deviations never exceed 5.1%, thus verifying the aforementioned robustness.

The mean adhesive force can also be calculated with the aid of probability distribution functions through the *continuous expression*

$$\overline{F}_{po} = \int_0^\infty \phi(F_{po}) F_{po} \, dF_{po} = \mu \,. \tag{8}$$

The drawbacks of this expression are connected to the assumption of log-normally distributed adhesive force as well as the determination of the unknown distribution parameters by least-square fitting to the experimental data. It is evident that the continuous expression corresponds to the $M \to \infty$, $N_{i+1} - N_i \to 0$ limits of the discrete expression.

In Fig. 6(a) and (b), the experimental mean adhesive force (discrete and continuous expressions) is compared to the van der Waals formula for the three nearly monodisperse dust populations and two dust deposition methods. A good agreement is observed for all dust sizes, as previously concluded in Ref. [20] but with far less statistics and less accurate (A, z_0) input. We note that the agreement is excellent for the 9 μm and 14 μm populations, whereas it becomes noticeably poorer for the 6 μm population. The latter highlights the need for empirical correlations that describe deviations from the van der Waals formula and will be explored in Section 3.4. However, in the case of fusion relevant dust-substrate combinations for which no adhesion measurements exist, the van der Waals formula still appears to be a useful zero-order approximation. It is also worth pointing out that the discrete and continuous expressions yield nearly identical results regardless of the dust size and deposition method, thus confirming the appropriateness of the log-normal distribution.

3.4. Empirical correlations for the mean and spread of the adhesive force

The predictive modelling of loss-of-vacuum-accidents in fusion reactors is carried out with numerical codes [47–49] whose dust remobilization modules are based on the Rock'n'Roll (R&R) dynamic resuspension model [38,39]. The R&R model assumes that the adhesive forces are log-normally distributed [38,39] and employs empirical expressions for the dependence of their mean and standard deviation on the dust size, the so-called Biasi correlations [39]. However, these correlations had been indirectly obtained by fine-tuning to resuspension measurements of different turbulent flow experiments and not directly established by best-fitting to adhesion measurements. Moreover, the utilized experiments employed dust grains of varying material composition (metal, metallic oxide and even organic). In addition, some of these experiments involved polydisperse populations and multi-layer configurations as well as provided poor information on the size ranges, sphericity, surface roughness and deposition method. Finally, we emphasize that the existence of global correlations is based on the implicit assumption that the effect of the surface roughness is strong enough to mask any sensitivity of adhesion to the dust or substrate material properties [50].

Tungsten is characterized by unusually high values of most physical properties that are important for adhesion (surface energy, Hamaker constant, mass density, Young's modulus). Hence, W-on-W adhesion should not be properly described by global expressions such as the Biasi correlations. This is confirmed by our experimental data, which can be employed to establish material-specific correlations. Since we have observed a strong dependence of adhesion on the deposition method (which will be investigated in Section 3.5), different empirical correlations will be provided. For *gas-assisted deposition*, we propose

$$\mu = 0.00452[1 + 29.920(D_d)^{0.288}]D_d, \quad (9)$$

$$\sigma = 0.00265[1 + 53.925(D_d)^{0.257}]D_d, \quad (10)$$

where μ, σ are expressed in μN and the dust diameter D_d in μm. For *gravity-assisted deposition*, we propose

$$\mu = 0.00086[1 + 52.432(D_d)^{0.503}]D_d, \quad (11)$$

$$\sigma = 0.00091[1 + 30.148(D_d)^{0.737}]D_d, \quad (12)$$

where again μ, σ are expressed in μN and D_d in μm.

The general form of the fitting functions $\mu, \sigma(D_d) = A[1 + B(D_d)^C]D_d$ was selected to be the same as in the Biasi correlations. As evident from Fig. 7, in spite of the fact that three-parameter fitting functions can be found that perfectly fit the limited datasets, the proposed correlations do not constitute perfect fits. Nevertheless, the recommended expressions are more physically extrapolated to larger and smaller sizes in contrast to perfect fits which either become negative or acquire unphysical maxima. Even though the proposed correlations constitute a W-specific improvement over the general Biasi correlations, it is evident that more data-points are necessary for more robust fits to be acquired. Therefore, any extrapolations should be carried out with caution and preferably restricted close to the 6–14 μm range of the data-points.

3.5. The dependence of the adhesive force on the dust deposition method

It is apparent from Table 1 and Figs. 6 and 7 that gas-assisted deposition results to much stronger W-on-W adhesion than gravity-assisted deposition. As described in Section 2.5, the basic difference between these two methods lies on the incident speed of the dust grain upon sticking on the substrate, whose average value is ~ 2.0 m/s for gas-assisted deposition and ~ 0.5 m/s for gravity-assisted deposition. For spherical W dust impinging on planar W substrates, the ratio of the yield velocity (minimum normal incident velocity for which the deformation induced by the impact energy is no longer purely elastic) over the adhesive velocity (maximum normal incident velocity for which an impact leads to zero rebound velocity) has been shown to be less than unity in the μm size range [10], implying that plastic deformation can take place during sticking impacts. Once the yield velocity ~ 0.1 m/s is exceeded, the extent of the contact area and thus the strength of adhesion will depend on the impact velocity. In gas-assisted deposition, higher impact velocities are achieved which lead to more extended plastic deformation and consequently to a higher mean adhesive force.

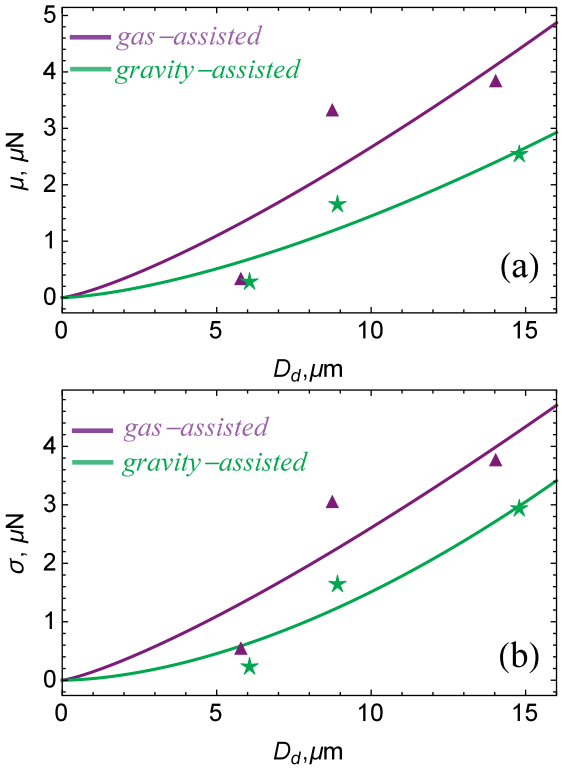

Fig. 7. The recommended analytic expressions for the size dependence of the (a) mean and (b) spread of the W-on-W adhesive force plotted together with the experimental data. The μ, σ experimental uncertainties are too small to be depicted on the graph in a meaningful manner: the relative deviations never exceed 5.1% and 7.2%, thus verifying the aforementioned robustness.

The observed dependence of adhesion on the deposition method has important implications. In facilities that replicate loss-of-vacuum-accidents [13,14] as well as laboratory tests of the efficiency of dust removal techniques [19], the deposition method is neither carefully controlled nor is it mimicking dust sticking as it occurs in tokamaks. This could influence both the repeatability of the experiments and limit their relevance to realistic tokamak conditions. We point out that, in contrast to our experiments which are focused on isolated grains, such experiments concern multilayers being focused on strong dust accumulation scenarios. However, the plastic deformation arguments presented above are valid not only for dust-substrate sticking impacts but also for dust-dust sticking impacts, since the underlying equations are the same after the introduction of an equivalent curvature radius [10].

4. Adhesive force distributions for tungsten dust deposited on beryllium-coated tungsten substrates

4.1. Motivation

In contemporary and future fusion devices with a beryllium first wall and a tungsten divertor (JET-ILW, ITER), a complete characterization of the adhesion between tungsten dust and beryllium substrates

is also important. To be precise, in such devices, parts of the divertor are covered by thin beryllium layers of varying thickness as a result of the well-studied global transport patterns of eroded beryllium atoms. Thus, inevitably, tungsten dust will be often adhered to a beryllium-coated tungsten surface [6,51,52].

From an electromagnetic viewpoint, the W-on-W non-retarded Hamaker constant is $A_{WW} = 4.98 \times 10^{-19}$ J and the W-on-Be non-retarded Hamaker constant is $A_{WBe} = 4.13 \times 10^{-19}$ J [46]. From a surface physics viewpoint, the W-on-W interface energy is $\Gamma_{WW} = 8.72\ J/m^2$ and the W-on-Be interface energy is $\Gamma_{WBe} = 5.65\ J/m^2$ [53]. Thus, the strength of both the instantaneous multipole interaction and the chemical bonding interaction (that ultimately result in adhesion) should observably but not drastically decrease as the tungsten surface gets gradually covered by a thin beryllium layer. However, the above theoretical arguments are valid for ideal surfaces. Hence, the main question that arises concerns whether the omnipresent structural, chemical, energetic heterogeneities will tend to mask or enhance the expected reduction of the adhesive force with increasing beryllium coverage. Aiming to address this question, dedicated electrostatic detachment experiments were carried out to quantify the adhesion of tungsten dust on beryllium-coated tungsten substrates (see Section 2.4 for technical details).

In the W-on-Be/W measurements, W dust was only adhered with the less time consuming gravity-assisted deposition method. Furthermore, in contrast to the W-on-W measurements where the goal was to describe the adhesive force distribution for a wide roughness range, the rms roughness of the Be/W substrate will be kept nearly constant while the coating thickness varies.

4.2. The measured adhesive force distributions

The adhesive force distributions for 9 and 14 μm nearly monodisperse spherical W dust adhered to Be-coated W substrates via the gravity-assisted deposition method are illustrated in Fig. 8. Apart from the three sets of W-on-Be/W measurements (δ = 10, 100, 1000 nm), a fourth reference set with the W-on-W measurements (δ = 0 nm) has been included in order to facilitate comparisons. For all combinations, the adhesive force approximately behaves as a log-normally distributed random variable. There is no systematic trend in the strength of adhesion as the coating thickness increases. In fact, it is evident that adhesion is barely affected by the presence of the beryllium coating, even for 1 μm thick Be films. This is verified by the mean and spread of the adhesive force provided in Table 2.

The only exception concerns the D_{nom} = 9 μm, δ = 100 nm measurements, which were also characterized by the worst quality least square fits to the log-normal distribution. This is visible in the low and high extraction force range of Fig. 8(a). This could be considered as a statistical fluke, since in the W-on-Be/W experiments the number of deposited dust grains is quite smaller than in the W-on-W experiments which makes the adhesive force more subject to fluctuations. On the other hand, the possibility of localized coating contamination and poor film quality present only for δ = 100 nm cannot be excluded. This is indirectly supported by the fact that the δ = 100 nm Be/W substrate also led to the strongest adhesion for D_{nom} = 16 μm (although it did not fluctuate as high as for D_{nom} = 9 μm). However, there were no direct optical evidence to reinforce such claim.

Overall, it can be concluded that the presence of thin Be coatings on W surfaces does not significantly modify the adhesion of W dust. The inability to detect any systematic dependence of adhesion on the coating thickness is not connected with the sensitivity limits of the measurement method but with the smoothing effect of the structural, chemical and energetic heterogeneities.

Table 2
Experimental results for the mean and spread of the adhesive force obtained for two nearly monodisperse populations (D_{nom} = 9, 14 μm) of spherical W dust adhered via gravity-assisted deposition to planar W substrates coated by Be layers of varying thickness (δ = 0, 10, 100, 1000 nm). Since multiple pure W substrates were employed for the W-on-W measurements (δ = 0 nm) that were characterized by different rms roughness, the equivalent rms substrate roughness $R_{q,\ eq}$ is provided that has been determined by the arithmetic average of each substrate roughness weighed by the relative number of detached dust grains.

D_{nom} = 9 μm					
δ(nm)	$R_{q,\ s}$(nm)	N	D_{avg}(μm)	μ(μN)	σ(μN)
0	51	3112	8.94	1.639	1.629
10	17	801	9.10	1.309	0.665
100	25	839	9.21	3.401	2.563
1000	26	713	9.22	1.774	1.530
D_{nom} = 14 μm					
δ(nm)	$R_{q,\ s}$(nm)	N	D_{avg}(μm)	μ(μN)	σ(μN)
0	53	714	14.82	2.493	2.825
10	17	260	14.95	2.681	2.388
100	25	333	15.21	3.032	3.196
1000	26	469	14.96	2.038	2.415

5. Summary and future work

The adhesive force measurements for spherical tungsten dust deposited on bulk tungsten surfaces and beryllium-coated tungsten surfaces have led to unambiguous conclusions courtesy of the very extended statistics obtained that consist of circa 20000 W grains detached

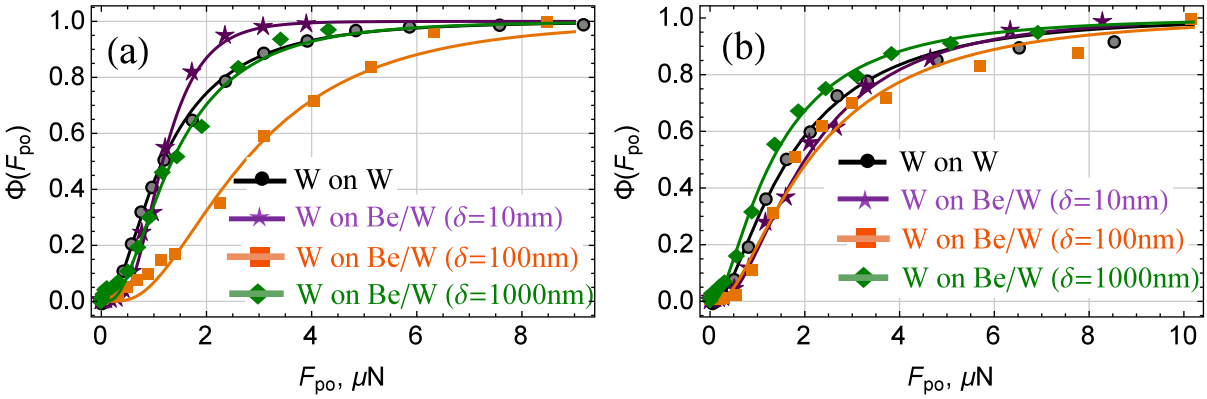

Fig. 8. The experimental cumulative probability distribution of the adhesive force (discrete points owing to the stepwise increase of the mobilizing electrostatic field) together with the least-square fitted log-normal cumulative probability (solid line) for the gravity-assisted deposition of spherical W dust on W substrates coated by Be layers of varying thickness (δ = 0, 10, 100, 1000 nm). Results for (a) D_{nom} = 9 μm, (b) D_{nom} = 14 μm.

from bulk W surfaces in the roughness range $R_{q,s} \sim 10 - 100$ nm and nearly 3500 W grains detached from Be-coated W surfaces for $R_{q,s} \sim 20$ nm: **(i)** Irrespective of the dust size and deposition method, the W-on-W adhesive force clearly behaves as a log-normally distributed random variable. **(ii)** Gas-assisted deposition (relevant for dust adhered to the tokamak first wall and divertor) systematically results to stronger W-on-W adhesion than gravity-assisted deposition (relevant for dust adhered to the vessel floor) owing to the onset of plastic deformation during sticking impacts. **(iii)** The van der Waals formula describes the mean W-on-W adhesive force only as a zero-order approximation. **(iv)** Empirical correlations are proposed that describe the size-dependence of the mean and standard deviation of the W-on-W adhesive force for each deposition method, they constitute input for the theoretical modelling of dust remobilization and resuspension. **(v)** The presence of thin Be coatings on W substrates does not significantly modify the adhesion of W dust, owing to the effect of the structural, chemical and energetic heterogeneities which tend to smooth out the reduction tendency stemming from the smaller Hamaker constant and surface energy of the W-Be system compared to the W-W system.

We point out that neither the dust grains nor the substrates involved in the electrostatic detachment measurements have been exposed to plasmas. Standard surface precleaning methods have been followed and the experiments have been performed in a low pressure chamber. Therefore, both the dust and the substrate surfaces should contain a respectable amount of adsorbates. This implies that the adhesive force measurements are subject to uncertainties due to chemical heterogeneities, which could influence both the mean and the spread of the adhesion. However, chemical heterogeneities are expected to be strongly reduced after exposure to plasma due to physical or chemical sputtering and/or desorption. The experimental quantification of the effect of plasma exposure on the W-on-W adhesive force will be the subject of future work.

Finally, it is worth emphasizing that, although far from atomically smooth, the substrates employed in these experiments were characterized by a relatively low degree of surface roughness ($R_{q,s} \sim 10 - 100$ nm), especially when compared with Be layers formed in tokamaks. The roughness of plasma-facing surfaces will strongly vary around the torus and most probably some regions will be characterized by higher roughness values due to non-uniformities in physical sputtering, material deposition and wall conditioning techniques (glow discharges, wall coating). Higher roughness degrees (up to the order of the nominal contact radius, $R_q \lesssim 1$ μm) should mostly affect the spread of the adhesive forces and less their mean value. For even higher roughness degrees (of the order of the dust radius, $R_q \gtrsim 1$ μm), the very definition of the adhesive force would be challenged, since it would no longer be possible to define a single surface normal at the length-scales of interest, multiple contact areas could be formed and a systematic configurational dependence would arise. In addition, reliable electrostatic detachment measurements would not be possible, since the exerted electrostatic force would no longer be described by the Lebedev formula and its magnitude would strongly depend on the configuration.

Acknowledgments

The authors would like to thank Matteo Pedroni for the surface roughness measurements. This work has been carried out within the framework of the EUROfusion Consortium and has received funding from the Euratom research and training programme 2014–2018 under grant agreement no. 633053. Work performed under EUROfusion WP PFC. The views and opinions expressed herein do not necessarily reflect those of the European Commission.

References

[1] J.P. Sharpe, D.A. Petti, H.W. Bartels, Fusion Eng. Des. 63–64 (2002) 153.
[2] J. Roth, E. Tsitrone, A. Loarte, et al., J. Nucl. Mater. 390–391 (2009) 1.
[3] S.I. Krasheninnikov, R.D. Smirnov, D.L. Rudakov, Plasma Phys. Control. Fusion 53 (2011) 083001.
[4] S. Ratynskaia, C. Castaldo, H. Bergsåker, D. Rudakov, Plasma Phys. Control. Fusion 53 (2011) 074009.
[5] M. Shimada, R.A. Pitts, S. Ciattaglia, et al., J. Nucl. Mater. 438 (2013) S996.
[6] X. Litaudon, et al., Nucl. Fusion 57 (2017) 102001.
[7] S. Ratynskaia, L. Vignitchouk, P. Tolias, et al., Nucl. Fusion 53 (2013) 123002.
[8] S. Ratynskaia, P. Tolias, A. Shalpegin, et al., J. Nucl. Mater. 463 (2015) 877.
[9] P. Tolias, S. Ratynskaia, A. Shalpegin, et al., Nucl. Mater. Energy 12 (2017) 524.
[10] P. Tolias, S. Ratynskaia, M. De Angeli, et al., Plasma Phys. Control. Fusion 58 (2016) 025009.
[11] S. Ratynskaia, P. Tolias, I. Bykov, et al., Nucl. Fusion 56 (2016) 066010.
[12] S. Ratynskaia, P. Tolias, M. De Angeli, et al., Nucl. Mater. Energy 12 (2017) 569.
[13] C. Bellecci, P. Gaudio, I. Lupelli, et al., Nucl. Fusion 51 (2011) 053017.
[14] S. Peillon, A. Roynette, C. Grisolia, F. Gensdarmes, Fusion Eng. Des. 89 (2014) 2789.
[15] M. Balden, N. Endstrasser, P.W. Humrickhouse, et al., Nucl. Fusion 54 (2014) 073010.
[16] A. Baron-Wiechec, E. Fortuna-Zalesna, J. Grzonka, et al., Nucl. Fusion 55 (2015) 113033.
[17] E. Fortuna-Zalesna, J. Grzonka, S. Moon, et al., Phys. Scr. T170 (2017) 014038.
[18] L. Begrambekov, A. Grunin, A. Zakharov, Nucl. Instrum. Meth. Phys. Res. B 354 (2015) 282.
[19] L.B. Begrambekov, A.N. Voityuk, A.M. Zakharov, J. Phys. Conf. Ser. 748 (2016) 012004.
[20] G. Riva, P. Tolias, S. Ratynskaia, et al., Nucl. Mater. Energy 12 (2017) 593.
[21] S. Peillon, M. Sow, C. Grisolia, F. Miserque, F. Gensdarmes, J. Electrostat. 88 (2017) 111.
[22] N.N. Lebedev, I.P. Skalskaya, Sov. Phys. Tech. Phys. 7 (1962) 268.
[23] W.R. Smythe, Static and Dynamic Electricity, Taylor & Francis, California, 1989.
[24] T.B. Jones, Electromechanics of Particles, Cambridge University Press, Cambridge, 1995.
[25] H.J. Butt, B. Cappella, M. Kappl, Surf. Sci. Rep. 59 (2005) 1.
[26] D.W. Cooper, H.L. Wolfe, Aerosol Sci. Technol. 12 (1990) 508.
[27] http://www.tekna.com/.
[28] P.L. Fauchais, J.V.R. Heberlein, M.I. Boulos, Thermal Spray Fundamentals, Springer, New York, 2014.
[29] J.J. Wang, J.J. Hao, Z.M. Guo, Y.M. Wang, Rare Met. 34 (2015) 431.
[30] Y. Sheng, J. Hao, Z. Guo, Adv. Mater. Res. 295–297 (2011) 135.
[31] X.L. Jiang, M. Boulos, Trans. Nonferrous Met. Soc. China 16 (2006) 13.
[32] C.P. Lungu, I. Mustata, V. Zaroschi, et al., Phys. Scr. T128 (2007) 157.
[33] C.P. Lungu, C. Porosnicu, I. Jepu, et al., Vacuum 110 (2014) 207.
[34] M. Götzinger, W. Peukert, Langmuir 20 (2004) 5298.
[35] T.T. Nguyen, C. Rambanapasi, A.H. de Boer, et al., Int. J. Pharm. 393 (2010) 88.
[36] S. You, M.P. Wan, Langmuir 30 (2014) 6808.
[37] K.L. Mittal, Particles on Surfaces I: Detection, Adhesion, and Removal, Plenum Press, New York, 1988.
[38] M.W. Reeks, D. Hall, J. Aerosol Sci. 32 (2001) 1.
[39] L. Biasi, A. de los Reyes, M.W. Reeks, G.F. de Santi, J. Aerosol Sci. 32 (2001) 1175.
[40] G. Ziskind, Rev. Chem. Eng. 22 (2006) 1.
[41] N.L. Johnson, S. Kotz, N. Balakrishnan, Continuous Univariate Distributions I, John Wiley & Sons, New York, 1994.
[42] J.N. Israelachvili, Intermolecular and Surface Forces, Academic Press, New York, 2011.
[43] H.C. Hamaker, Physica 4 (1937) 1058.
[44] D. Tabor, J. Colloid Interface Sci. 58 (1977) 2.
[45] L.H. Lee, Fundamentals of Adhesion, Springer Science, New York, 1991.
[46] P. Tolias, Fusion Eng. Des. (2018).
[47] S. Paci, F. Parozzi, M.T. Porfiri, Fusion Eng. Des. 75–79 (2005) 1243.
[48] A. Rondeau, J. Merrison, J.J. Iversen, et al., Fusion Eng. Des. 98–99 (2015) 2210.
[49] F. Tieri, F. Cousin, L. Chailan, M.T. Porfiri, Fusion Eng. Des. 124 (2017) 1287.
[50] M.P. Kissane, F. Zhang, M.W. Reeks, Nucl. Eng. Des. 251 (2012) 301.
[51] Y. Ueda, J.W. Coenen, G. De Temmerman, et al., Fusion Eng. Des. 89 (2014) 901.
[52] S. Brezinsek, A. Widdowson, M. Mayer, et al., Nucl. Fusion 55 (2015) 063021.
[53] L. Vignitchouk, P. Tolias, S. Ratynskaia, Plasma Phys. Control. Fusion 56 (2014) 095005.